

A Coupled Hydro-Mechanical Analysis to Investigate the Behavior of a Monitored Slope under Transient Rainfall

Un análisis hidromecánico acoplado para investigar el comportamiento de una pendiente monitoreada bajo precipitaciones transitorias

Dr. L. Sebastian Bryson & Dr. Daniel Francis Civil Engineering, University of Kentucky, United States of America

Faisel Ahmed Staff Geotechnical Engineer, PanGeo, Inc., United States of America

ABSTRACT: Shallow planar landslides induced by rainfall events are common in steep topography consisting of weak colluvial soils. Few studies have been reported that show the rainfall threshold at the point at which a distinct shift in mechanical behavior from static to dynamic conditions is observed. In general, a direct behavioral response between soil hydrologic behavior and slope deformation by applying coupled hydro-mechanical process is poorly understood. The purpose of this work is to evaluate the hydro-mechanical behavior of a studied slope during and after a period of transient rainfall. This purpose was achieved by evaluating the deformability changes during the change in water content of the soil mass of a slope. The slope was at the site of a previous landslide. The slope was modeled using a finite element program and calibrated to match site conditions using on-site soil hydrological and deformability properties. Coupling the hydrologic and mechanical behavior of the soil revealed that a behavioral transition occurred at a specific cumulative infiltration level, resulting in saturation. The coupled behavior exhibited a parallel response during the drying and wetting stages. When approaching the specific cumulative infiltration, the site's mechanical behavior shifted significantly. The volumetric water content of the soil and the deformation behavior during various rainfall events served as the framework of the study.

KEYWORDS: rainfall; slope deformation; landslide; hydro-mechanical; finite element;

1 INTRODUCTION

Shallow planar landslides induced by rainfall events are common in steep topography consisting of weak colluvial soils (Montrasio and Valentino 2008; Wu et al. 2018). The hydrologic and mechanical behavior of a rainfall-induced shallow landslide has been studied extensively (Iverson 2000, Zhan et al. 2013; Zhuang et al. 2017; Hoang and Bui 2018; Crawford et al. 2019). These researchers considered mechanical and hydrological behavior of soil mass, as independent triggers of landslides. However, several researchers (Wu et al. 2018; Zhang et al. 2019; Wei et al. 2020; Liu and Wang 2021) have emphasized the importance of the coupled hydro-mechanical behavior in analyzing rainfall-induced shallow landslides.

The viability of utilizing coupled hydro-mechanical behavior for rainfall-induced landslide prediction has been demonstrated by several researchers (Soga et al. 2016; Gao et al. 2017; Tang et al. 2017; Schulz et al. 2018; Tang et al. 2019; Yang et al. 2020; Wu et al. 2020). Although the concept of rainfall threshold in predicting slope failure during a transient event has been studied (Marin and Velásquez 2020; Kim et al. 2021; Distefano et al. 2022; Rana and Babu 2022; Yuniawan et al. 2022), few studies have been reported that show the rainfall threshold at the point in which a distinct shift in mechanical behavior from static to dynamic conditions are observed. In general, a direct behavioral response between soil hydrologic

behavior and slope deformation by applying coupled hydro-mechanical process is poorly understood. The purpose of this work was to evaluate the hydro-mechanical behavior of a studied slope during and after a rainfall season. This purpose was achieved by evaluating the deformability changes during the change in water content of the soil mass of a slope.

The study was based on a previous work by Crawford et al. (2019) that monitored a site of a previous landslide for two years. During this time, the site experienced seasonal stages of drying and wetting. Hydrologic and deformation sensors were installed to record fluctuations in slope hydrology and soil displacement at the toe of the landslide. However, changes in stresses and deformations with respect to time are required to fully understand the slope's hydro-mechanical response to transient rainfall.

Hence, our study additionally assessed the relationship between mean effective stress and suction stress. However, the site only offered data on the volumetric water content of the soil and slope deformation. As a result, a finite element analysis was used to model the field slope to obtain additional data on soil hydrologic and deformation response. Hydrologic and deformability field data were used to define the input of the finite element analysis. The output was evaluated to draw consistent conclusions. The analysis demonstrated that the coupled hydro-mechanical behavior of a site was affected during different stages of a season. The seasonal analysis showed that the



hydrologic variability and the deformational characteristics of the slope were particularly acute during the wetting season. Therefore, this study concentrated on analyzing data collected during a wetting season. The intent of the study was to better understand the hydro-mechanical coupling that occurred in a slope under transient rainfall conditions.

2 PROJECT FIELD SITE

The slope monitoring was performed at the site of the Roberts Bend landslide, which is in Pulaski County, Kentucky. Data collected by Crawford et al. (2019) from 10/22/2015 through 10/12/2017 was used as the basis for the hydro-mechanical analyses in this study. The potential major cause of instability was a shallow planar failure located in the interphase between the colluvial soil and the bedrock. But there are also small rotational landslides. Figure 1 shows an aerial picture of the landslide site, along with the location of the site relative to the State.

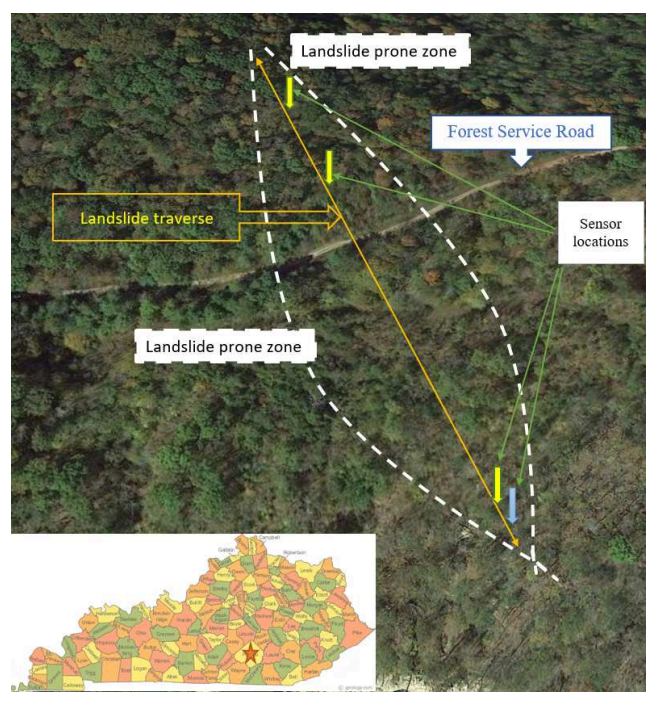


Figure 1. Aerial picture of Roberts Bend landslide. Orange line defines the monitoring trajectory of the slope, yellow arrows show the location of hydrologic sensors, and the blue arrow shows the location of CET sensor.

Crawford et al. (2018) and Crawford et al. (2019), presented a geophysical and geotechnical assessment of the geologic and geomorphic site characteristics at the Roberts Bend landslide and therefore will not be repeated here. In general, the site was approximately 1.5 m to 3.5 m of silty clay colluvium underlain by a weathered clay-shale. The bedrock at the site consists of clay-shale with sandstone, limestone, dolomite, and siltstone interbeds. A U.S. Forest Service gravel road crosses the slope about 2/3 upslope (see Figure 1). The geological and geotechnical characteristics of the landslide vary above and below

the service road. Crawford et al. (2019) reported above the service road, the landslide features were somewhat subdued, except for a prominent headscarp that defined the upper extent of the landslide area. Below the service road, the landslide had well-defined scarps, distinct flank features, hummocks, and a toe bulge.

2.1 Field-Hydro Mechanical Data

Field hydrologic data at Roberts Bend were measured using two types of hydrologic sensors. A Campbell Scientific CS655 water content reflectometer was used to measure in-situ soil volumetric water content and a Decagon MPS-6 water potential sensor was used to measure soil suction. The hydrologic sensors were installed in pits at upslope, mid-slope, and downslope areas of the landslide complex. The sensors were placed at different depths depending on the soil horizons. The downslope hydrologic sensors were placed at 25 cm and 44 cm below the slope surface as seen in Figure 2. The soil sensors were nested vertically, creating a pair of each at one soil horizon. Mid-slope and upslope data were not utilized for the current study. The reason being the downslope soil hydrologic sensors were in the proximity of a cable-extension transducer (CET). The CET was located at the downslope pit, as shown in Figure 2, and was used to measure slope movement. The CET was a stainless-steel cable that measured absolute linear displacements. One end of the CET system was located on an assumed stable part of the slope. The cable stretched from the stable part of the slope where it was anchored to a pole in the ground. The proximity downslope soil hydrologic sensors and the CET enabled the simultaneous observation of changes in soil hydrologic and deformation behavior as a function of transient rainfall. Rainfall was measured using a tipping bucket rain-gauge and Rainlog 2.0 data logger. The logger had a 1-minute resolution, and the rain gauge was calibrated at 0.25mm/tip. The soil hydrologic data and the CET data from the sensors were collected using a Campbell Scientific CR1000 data logger with an external power supply system. Sensor data was retrieved in 15-minute, hourly, and daily average value tables. This study used daily data to examine seasonal soil hydrologic response and slope movement.

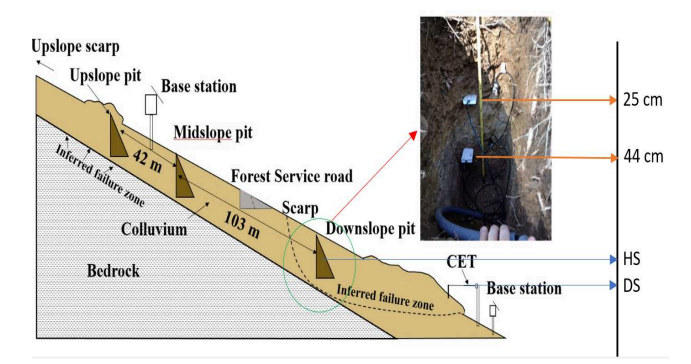


Figure 2. In-situ instrumentation for Roberts Bend slope (after Crawford et al. 2019). In the figure, "HS" indicates the location of the hydrologic sensors and "DS" indicates the location for the deformation sensor.



2.2 Soil Volumetric Water Content and Soil Suction Data

As was previously mentioned, field testing at Roberts Bend was examined from a two-year period. From an analysis of the data presented by Crawford et al. (2019), it was observed that significant changes in hydrologic and mechanical measurements occurred over a one-month time frame during the wetting season, from 11/29/2016 to 12/29/2016. Thus, this study focused the analysis on this time frame. Figure 3 presents the rainfall and hydrologic data [i.e., volumetric water content data (VWC) and soil suction data] measured during the one-month analysis time frame.

Figure 3(a) shows the measured VWC data for 25 cm and 44 cm for the site, superimposed onto the rainfall data. Figure 3(a) shows the VWC is higher at the deeper depth, but also the VWC changes slightly faster at the shallow depth. This behavior can be explained as a logical consequence of the shallow depth wetting and drying faster than 44 cm depth. This was reflected in the beginning of the soil VWC plot for 25 cm and 44 cm. The beginning VWC for 25 cm was 0.17 and beginning VWC for 44 cm was 0.41. With respect to the one-month observation period, it was observed that the 25 cm VWC data changed at an average rate of 0.0041 per day. The average rate of change for the 44 cm VWC data was approximately 0.0018 per day. From Figure 3, it was observed there were six days of heavy rainfall that corresponded with noticeable response changes in the VWC sensors. These six days were 11/30/16, 12/06/2016, 12/12/2016, 12/18/2016, 12/24/2016, and 12/27/2016. These days had rainfall greater than 20 mm [marked with arrows in Figure 3(a)].

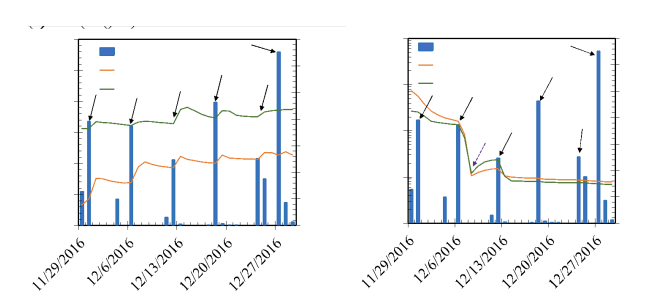


Figure 3. In-situ measured data for Roberts Bend from 11/29/2016 to 12/29/2016 at the downslope pit (a) soil volumetric water (b) soil suction (after Crawford et al. 2019).

The soil suction data for Roberts Bend during one-month observation period at 25 cm and 44 cm is shown in Figure 3(b). The field soil suction started from 729 kPa for the 25 cm depth. For the 44 cm depth, the suction started at 267.4 kPa. Figure 3(b) shows that from 11/30/2016 to 12/06/2016, soil suction decreased at the 25 cm and 44 cm depths, by an average of 77.9 kPa to 20.5 kPa per day, respectively. Between 12/06/2016 and 12/08/2016 [marked dashed arrow in Figure 3(b)], both 25 cm and 44 cm were wetting at almost equal rates. This was assumed to indicate absolute downward flow of water due to inflow being greater than outflow. Between 12/08/2016 and 12/12/2016, both 25 cm and 44 cm depths were drying. This was due to the lack of rainfall between these dates. On these dates, the drying soil suction at the 44 cm depth was an average of 2.85 kPa per day. The average

drying soil suction for the 25 cm depth during this period was approximately 1.2 kPa per day. As can be seen, the average of drying soil suction at 44 cm was more than twice that of the 25 cm depth. This could be due to different hysteretic responses at the two depths. The hysteretic response is defined herein as the retardation of soil suction response caused by the forcing function changing from drying to wetting. The hysteretic response is a function of the stress history and the initial state (e.g., density and water content) of the soil. By definition, the soil at a 25 cm depth will have a slightly different stress history and initial state than the soil at the 44 cm depth. After 12/12/2016, both soils at 25 cm and 44 cm started to saturate due to the rainfall at the mentioned date. After 12/14/2016, both the soil suction at 25 cm and 44 cm had reached below 9 kPa. The in-situ soil suction sensor measurement limit of 9 kPa. As a result, any measured soil suction less than 9 kPa was assumed not to be valid.

2.3 Slope Deformation Data

The slope deformation data for Roberts Bend at the downslope pit location is shown in Figure 4. The data is shown from 11/17/2106 through 04/17/2017.

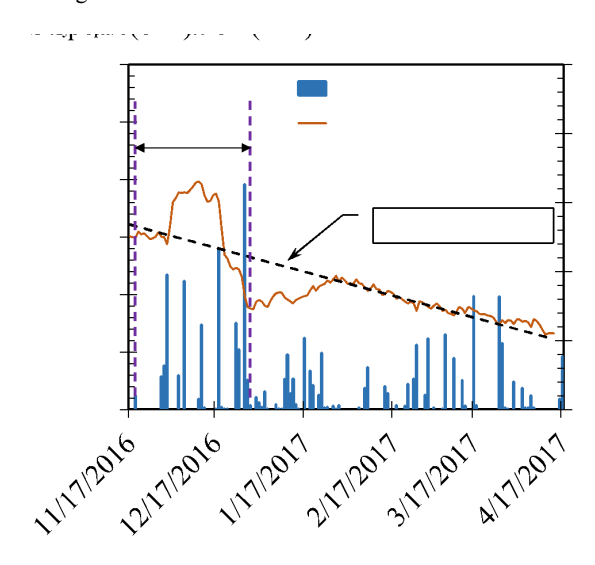


Figure 4. Slope deformation data for Roberts Bend from 11/17/2016 to 4/17/2017

Crawford et al. (2019) outlined how CET determined displacement. The CET was used to determine the extension and retraction motions of a linear stainless-steel cable. The CET can only be positioned linearly along a horizontal line. The deviations from shortening (positive movements in Figure 4) can be attributed to a variety of factors including: bulging of the anchor pole as a result of ground rotation, temperature changes in the cable over time, and ground rotation that led the CET pole to rotate forward (Crawford et al. 2019). The displacements measured by the CET were assumed to be caused by the sliding of the whole colluvial layer along the top surface of the bedrock. This assumption supports the possibility that the anchor pole experienced some rotation. Although the possibility of the anchor pole rotating with movement of the soil mass precludes absolute



displacement measurements, the brief observations of "apparent" upward slope movement are peripheral and can be considered inconsequential with respect to the general slope moving direction.

The trend of the slope movement during the wetting season was considered following the trendline shown in Figure 4. The rate of downslope movement indicated by the linear trendline shown in Figure 4 is roughly 0.13 mm per day.

2.4 Site Precipitation Data

As was previously mentioned, the in-situ rainfall data for Roberts Bend was obtained by a rain gauge. The evapotranspiration data for Roberts Bend during the analysis period was obtained from the Irrigation Manager System (IMS) operated by the Kentucky Mesonet system for the National Weather Service (http://weather.uky.edu/php/cal_et.php). The IMS requires the county location as well as the analysis period for the desired site to provide evapotranspiration data. Unfortunately, Roberts Bend is in Pulaski County and was not available from IMS. As a result, evapotranspiration data was obtained from Lincoln County, a county adjacent to Pulaski County. Figure 5 shows the rainfall and evapotranspiration data used for this study. In the figure. cumulative data for "R", "ET", and "I" represent rainfall, evapotranspiration, and infiltration, respectively. In Figure 5, the R data are "positive precipitation", and the E data are "negative precipitation". During the analysis, no surface runoff was assumed. Therefore, the infiltration "I" represents the net flux of rainfall and evapotranspiration.

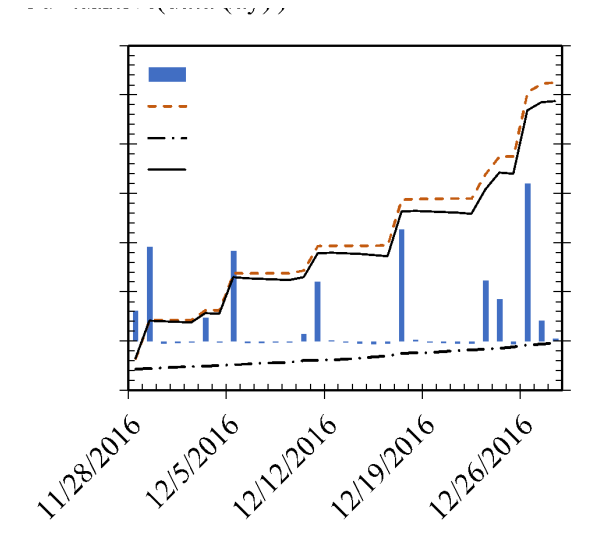


Figure 5. Site precipitation data along with cumulative rainfall, cumulative evapotranspiration, and cumulative infiltration for Robert's Bend

Behavior of cumulative "I" was closer to the behavior of cumulative "R" than it was to cumulative "ET" during this rainy period. The inclusion of "ET" data is crucial in analyzing soil hydrologic behavior (Ahmed et al. 2021). Using an analytical transient infiltration model, Ahmed et al. (2021) predicted the

seasonal change of in-situ soil hydrologic behavior. Ahmed et al. (2021) performed analyses that compared the transient performance of hydrologic analytical model using no "ET", one average "ET" and variable "ET" data. Ahmed et al. (2021) demonstrated that including the variable "ET" gave a better performance to the analytical transient infiltration model. Therefore, including the transient "ET" data with the "R" data will be used in the current study for the soil hydrologic and displacement analysis during the analysis period at Roberts Bend.

2.5 Soil Hydrologic and Geotechnical Data

The soil data for Roberts Bend was obtained using the Web Soil Survey (WSS) soil database. (https://websoilsurvey.nrcs.usda.gov/app/) The WSS is operated by the U.S. Department of Agriculture (USDA), Natural Resource Conservation Service (NRCS) and provides soil data for greater than 95 percent of the United States counties. These data are often used to supplement data from in-situ soil testing, In-situ geotechnical data were not available at the Roberts Bend site, which necessitated the use of WSS data. Depth to bedrock at the Roberts Bend landslide was approximately 3 meters at the downslope location (Crawford et al. 2019). The van Genuchten (1980) hydrologic model was used to approximate the Soil Water Characteristics Curve (SWCC). The van Genuchten (1980) model is described as Equation 1:

$$S_e = \left(1 + (\alpha \psi)^n\right)^{-m} \tag{1}$$

where, S_e = the effective degree of saturation; ψ = soil suction; α , n,m are soil fitting parameters. $S_e = \frac{\left(\theta - \theta_r\right)}{\left(\theta_s - \theta_r\right)}$; θ , θ_s , θ_r are the current volumetric water content, saturated volumetric water content, and residual water content, respectively. Estimates of fitting parameters to evaluate suction of this soil were obtained with the aid of the software Rosetta lite v.1.1 from Hydrus-1D (Šimůnek et al 2016). As an output, Rosetta provided the van Genuchten (1980) hydrological model fitting parameters (α ,n)

and saturated hydraulic conductivity (k_s) , the van Genuchten

(1980) fitting parameter m was approximated as $1 - \frac{1}{n}$ (Mualem 1976). The hydrological and geomechanical parameters used for developing a coupled model for the site are presented in Table 1. The geomechanical data were obtained from the Crawford et al. (2019), the WSS data, and assumed typical values. The data are given at the depth corresponding to the upper depth of the nested sensors (25 cm), the lower depth of the nested sensors (44 cm), and the average depth corresponding to the top of bedrock (300 cm)

Table 1. Physical and mechanical properties of the in-situ soil at different layers

14 / 015			
Soil property	25 cm	44 cm	300 cm
% Sand	29	18	34
% Silt	53	54	38



% Clay	18	28	28
Bulk Density, ρ (gm/cm³)	1.3	1.35	1.65
α (kPa ⁻¹)	0.056	0.071	0.13
n	1.65	1.18	1.36
θ_s	0.42	0.52	Not required
θ_r	0.064	0.081	Not required
k _s (cm/day)	26.9	14.3	Non-porous
Unit Weight, γ (kN/m³)	17	18	19
Initial Void Ratio, e ₀	0.52	1.08	0.5
Elastic Modulus, <i>E</i> (kPa)	64,000	66,000	$4x10^{6}$
Poisson Ratio, v	0.3	0.3	0.3
Cohesion Intercept, c' (kPa)	12	15	200
Soil Friction Angle, φ' (deg)	22	25	45

2.6 Soil Layer Distribution and Water Table Location

The analysis focused on the data from the downslope location, below the forest service road. The thickness of the colluvium varied from 1.5 m at the top of the slope, to 3.5 m at the bottom of the slope. The slope angle was approximately 18 degrees with respect to the horizontal. The location of the water table was not exactly known. Therefore, the water table location was found by back calculation from the soil hydrologic sensor readings. Converting volumetric water content to degree of saturation ($S = \frac{\theta}{\varphi}$: where S = degree of saturation; $\varphi =$ porosity, which is a function of void ratio), information of the degree of saturation at depths of 25 cm and 44 cm, were observed to be 0.44 and 0.79 respectively. These data were used to create a hypothetical hydrostatic pressure distribution line (HPDL) assuming a linear hydrostatic distribution. This is presented in Figure 6. From the HPDL, a degree of saturation of 1.0 was projected at the 55 cm depth. Therefore, the 55 cm depth below the ground surface was taken as the location of the water table. The water table was assumed to be static and uniform along the slope surface.

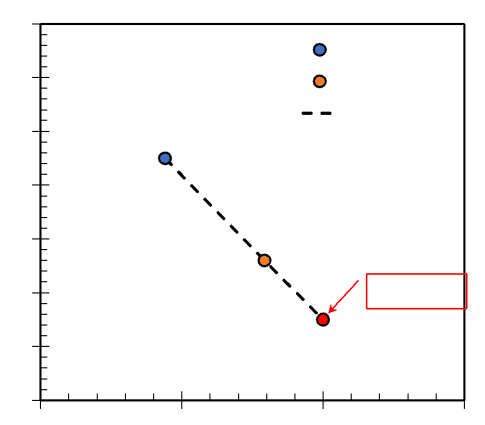


Figure 6. Hydrostatic pressure distribution line (HPDL) for Roberts Bend

3 FINITE ELEMENT ANALYSIS

3.1 FEM Model Setup

The Plaxis 2D finite element software (Bentley Systems, Inc., https://www.bentley.com/software/plaxis-2d/) was used to model the coupled hydro-mechanical behavior involved in the slope analysis. The finite element model (FEM) facilitated the determination of deformations as well as changes in effective stresses that resulted from changes in the hydrologic regime. Once calibrated, the FEM alos allowed for behavior to be estimated at depths other than the the locations of sensors. The slope FEM for Roberts Bend is presented in Figure 7. The figure shows the 2D geometry of the slope and the generated mesh for the finite element analysis. The geometry is presented in units of "meters".

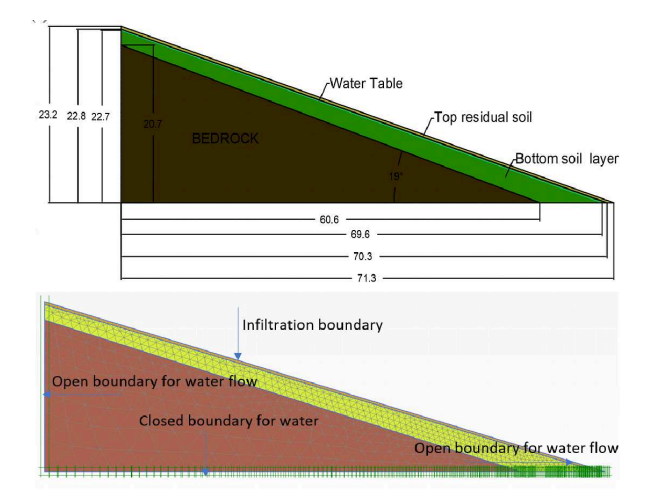


Figure 7. Finite element model for the slope: (a) Geometry of the slope model in PLAXIS (b) Mesh plot with water boundaries of the slope model in PLAXIS.



In Figure 7(a), a small layer in the slope surface, which was called the "residual layer" to indicate the colluvial material that is most likely undergoing a weathering process, has an average thickness of 44 cm. The "bottom soil layer", with a thickness of 210 cm, is the soil in contact with bedrock. The water table is located within the bottom soil layer as shown in Figure 7. For developing the FEM, a 15-noded plane strain element was adopted. The mesh coarseness factor considered for bedrock, bottom soil layer and top residual layer were 1.0, 0.4 and 0.3, respectively. A finer mesh was used for top layer because the slope deformation was measured within the top layer. The number of elements generated by mesh assignment was 1505. The element distribution for mesh assignment was considered medium, as defined by Plaxis. The plot with mesh elements is shown in Figure 7(b). Standard fixities were applied in analyzing the slope model. The bottom of the slope model was completely fixed, the sides were normally fixed, and the top was fully free. The infiltration boundary of the model was the top surface. The water within the model was allowed to flow from all sides except the bottom. The Mohr-Coulomb model was adopted for defining all the soil properties. Since the analysis was performed for one complete month of the wetting season, the drainage type for both residual layers were considered at drained condition. The bedrock was assumed to be non-porous.

3.2 FEM Initialization

To analyze the coupled behavior for Roberts Bend in the FEM, it was necessary to calibrate the model based on in-situ sensor readings. An initial phase (i.e., pre-analysis period) was developed for the FEM prior to performing the actual analysis. The initial phase was defined with gravity loading and a phreatic-type pore pressure. After finishing this initial step, the FEM output presented the maximum suction value of 5.6 kPa. However, this initial suction from the FEM did not match the soil suction readings from the in-situ sensor measurements. The in-situ initial soil suction sensor reading at 25 cm and 44 cm, for the period from 11/29/2016 to 12/29/2016 were 729.1 kPa and 267.4 kPa, respectively. As a result, it was assumed reasonable to calibrate the pre-analysis period of the FEM using in-situ values taken near the surface. Hence, the in-situ soil suction sensor reading at 25 cm was selected to match with the pre-analysis period in PLAXIS. Also, steady state had to be ensured in the period of 11/29/2016 to 12/29/2016. To achieve a steady state with a fully coupled flow deformation behavior, an evapotranspiration rate of 0.05 m per day was applied. This was necessary to achieve the target initial soil suction of 729.1 kPa at 25 cm. The evapotranspiration rate was applied for pre-analysis period of 800 days. This period was found by trial and error. The result is shown in Figure 8.

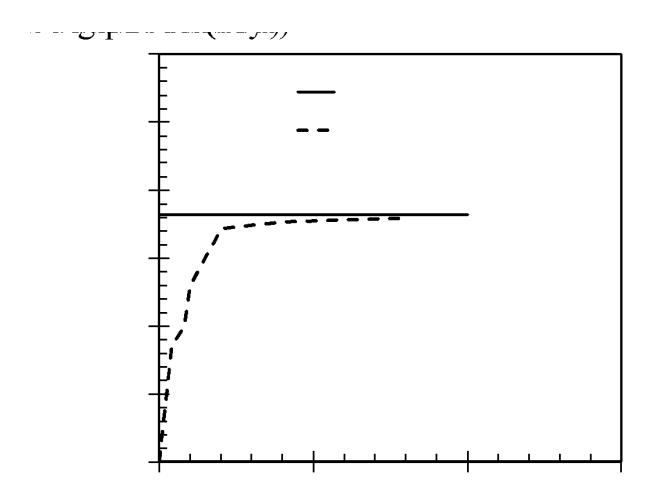


Figure 8. Soil suction reading at 25 cm from PLAXIS at different phases of the pre-analysis period of 11/29/16 to 12/29/16

Figure 8 shows the soil suction at 25 cm achieved a steady value of around 717 kPa at a pre-analysis period of 800 days with 0.05 m per day evapotranspiration rate. The steady state analysis was completed in forty subsequent phases. Each phase ran for 20 days due to numerical convergence issues. Hence, the slope model in PLAXIS was considered to achieve actual in-situ steady state after the 800-day period.

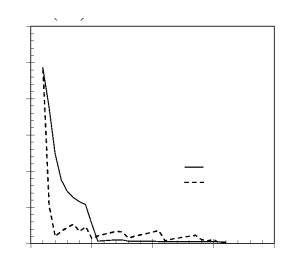
It is acknowledged that the required steady state condition can also be achieved with different evapotranspiration rates and different periods. An analysis to determine "which evapotranspiration rates and periods" produced "which steady state conditions" was beyond the scope of the study and hence, was not performed.

3.3 Model Validation Against Measured Field Data

3.3.1 Performance of Soil Suction Modeling

After the pre-analysis period, the FEM was run for thirty days and the results were compared to the measured infiltration data as shown in Figure 3. For the FEM, each day of rainfall and evapotranspiration was set as an individual phase in the FEM run. Here, one day of a rainfall/evapotranspiration event was considered as one single phase in the FEM analysis. Therefore, for the thirty days of infiltration, thirty separate phases were created for the FEM slope model. The soil hydrologic data from 25 cm and 44 cm were taken from the FEM once the model run was completed. Figure 9 shows the measure and predicted soil suction at 25 cm and 44 cm, respectively.





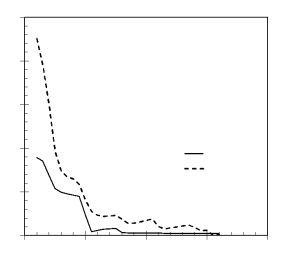


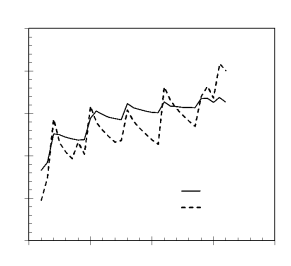
Figure 9. Measured and predicted soil suction for Roberts Bend: (a) data at 25 cm depth; (b) data at 44 cm depth.

For the soil suction reading at 25 cm from Figure 9(a), it was observed that the rate of soil suction decrease (due to saturation) for the measured data was higher than that for the predicted data. The predicted soil suction for 25 cm dropped to 28 kPa on 11/30/2016 from 717.1 kPa. The measured soil suction at the same date dropped to 372 kPa. The infiltration rate on 11/30/2016 was -1 mm, which signifies evapotranspiration. However, the infiltration rate on 11/29/2016 was 38.5 mm indicating rainfall. It was speculated that the saturated hydraulic conductivity, $k_{\rm s}$, from field data, caused faster saturation for the PLAXIS data compared to the measured data on 11/30/2016. Higher $k_{\rm s}$ values tended to

regulate moisture flow (Wildenschild et al. 2001). This caused the predicted data to reach near saturation on 11/30/16. The measured data reached near saturation on 12/07/16. The in-situ soil suction sensors had a measuring limit of 9 kPa. Therefore, any soil suction data less than 9 kPa could not be validated. For the soil suction reading at 44 cm from Figure 9(b), it was observed the rate of decrease in soil suction for measured and predicted were approximately equal. The measured data for 44 cm started from an initial value of 267.4 kPa. Results from the predicted model show an initial value of 676.9 kPa. Despite this difference in the initial data, Figure 9(b) showed the PLAXIS model behavior was in good agreement with the field response. Both the measured and the predicted data at 44 cm reached near saturation on 12/07/2016.

3.3.2 Performance of Volumetric Water Content Modeling The soil volumetric water content at the 25 cm and 44 cm depths in the downslope pit is shown in Figure 10. The FEM model data at 25 cm had a similar behavior as the measure data, according to Figure 9(a). At a depth of 25 cm, a noticeable fast rise and fall in volumetric water content data was seen for both measured and predicted data sets. Even though the behavior of the curve is not smooth, the general trend of the curve is clear. This can be explained by the proximity of the sensor to the surface, where sensitivity to rainfall and evapotranspiration is higher. The soil at 25 cm became wet and dry quickly during the wetting and drying cycles. Therefore, the quick response during wetting and drying cycles generated the zigzag pattern shown in Figure 10(a) for 25 cm. The change in response was much more abrupt for the predicted data compared to the measured data at 25 cm. As discussed previously, it was assumed the predicted soil hydraulic conductivity at 25 cm generated the observed behavior. The plot for 44 cm from Figure 10(b) shows the predicted data behaved differently compared to the measured from 11/28/2016 to

12/11/2016. The starting volumetric water content for the predicted and measured was 0.3 and 0.4, respectively. Hence, the predicted data started at a much drier state compared to the measured at 44 cm.



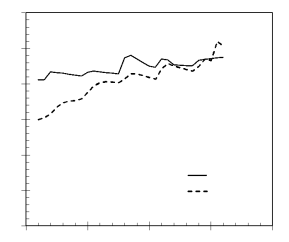


Figure 10. Measured and predicted volumetric water content for Roberts Bend: (a) data at 25 cm depth; (b) data at 44 cm depth.

The influence of moisture content in the hydro-mechanical behavior of soils can be explained in terms of the Soil Water Characteristic Curve (SWCC) developed from the data presented previously in Table 1. Figure 11 presents the full SWCC (i.e., from saturated conditions to dry conditions) used for this study. In Figure 11, Point M represents the starting point for the predicted hydrologic data that corresponds roughly to from 11/29/2016 and to Point N represents starting point for measured hydrologic data.

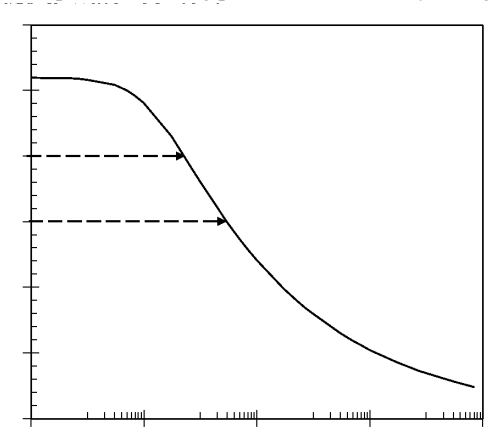


Figure 11. Soil Water Characteristic Curve "SWCC", 44 cm depth at Roberts Bend landslide

From Figure 11, Point M experienced an initial steeper rise compared to Point N. Therefore, the rise from Point M was faster compared to Point N. This behavior was observed in Figure 10(b) for 44 cm from 11/28/2016 to 12/11/2016. Overall, the predicted soil hydrologic data for 25 cm and 44 cm from PLAXIS demonstrated consistent results with the measured in-situ data.

3.3.3 Slope Deformation

The predicted and measured slope deformation information for Roberts Bend is shown in Figure 12. On 12/27/2016, the predicted data showed a higher displacement of 40.4 mm



compared to the measured data. A possible explanation for this behavior can be posited from investigating the field data in Figure 12, the displacement data up to 3 mm was displayed with a break line for illustration purposes.

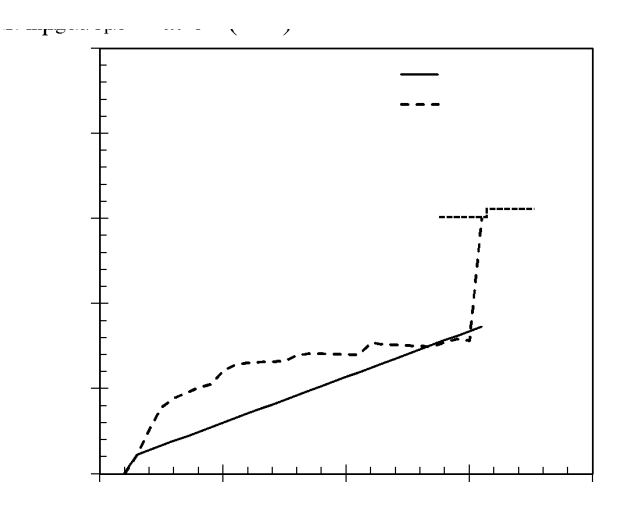


Figure 12. Slope deformation for Roberts Bend at near surface.

Figure 12 showed the FEM predicted higher slope displacements compared to the measured displacements. An initial general trend was considered for practical purposes. This straight line is the measured data shown in Figure 12. Along with the predicted deformation plot, the data showed variable rates of increase. For example, from 11/29/2016, to 12/01/2016, the deformation rate was 0.27 mm (average) per day. From 12/02/2016 to 12/05/2016, the deformation rate was 0.07 mm (average) per day. This was when little or, no rainfall was observed compared to the initial wetting phase from Figure 5. From 12/05/2016, to 12/07/2016, the deformation rate began to rise at an average rate of 0.12 mm per day. This was due to the rise in rainfall as seen in Figure 5 at the corresponding dates. Overall, the slope deformation response was consistent to days of rainfall and no rainfall.

4 COUPLED HYDRO-MECHANICAL BEHAVIOR ANALYSIS

The FEM was initially calibrated from in-situ hydrologic and deformation sensor readings. The comparison between the numerical method and the field data is consistent. During the initialization phase, a hydrologic regime was developed. The regime showed a good match with the 25 cm, 44 cm sensor depths. The in-situ surface deformation matched well with the FEM. For the in-situ soil hydrologic data, the areas of high and low moisture content identified by Crawford et al. (2019) corresponded very well to areas of high and low moisture content observed in the FEM model. Therefore, the model was assumed to be valid throughout the soils profile, down to the soil-bedrock interface. Under this assumption, extended hydro-mechanical

behavioral analyses were performed for the slope system during a complete month of the observation period.

4.1 Hydro-Mechanical Behavioral Analysis at 25 cm

Figure 13 shows the deformation plot with volumetric water content for Roberts Bend at 25 cm. It presents the drying and wetting paths. Drying phases were considered in days absent of rainfall during the wetting season analysis period. When the wetting phase reached Point A, the soil volumetric water content was approximately 0.4. The saturated volumetric water content at 25 cm was 0.42. The cumulative infiltration at the date occurring at Point A was approximately 165 mm. Therefore, at 165 mm of cumulative infiltration, the soil at 25 cm reached very near to saturation. After Point B, when the site experienced a wetting phase, the wetting path line broke at C and caused a higher shift compared to BC. Along BC, the average rate of rise was 1.5 mm per day. The subsequent wetting path starting from C experienced an average rise of 5.1 mm per day.

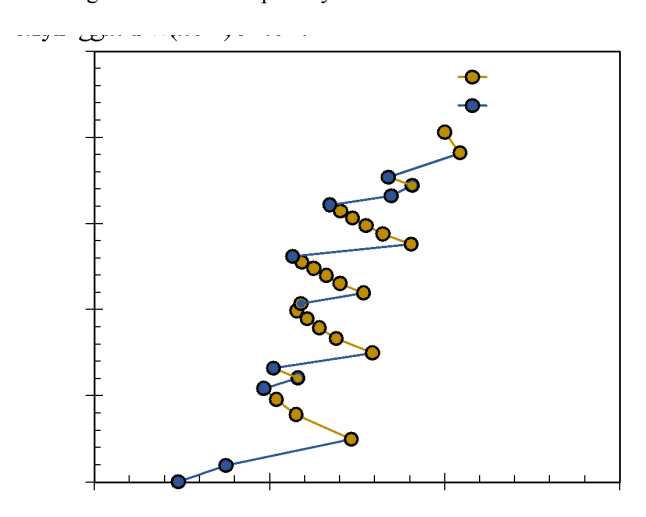
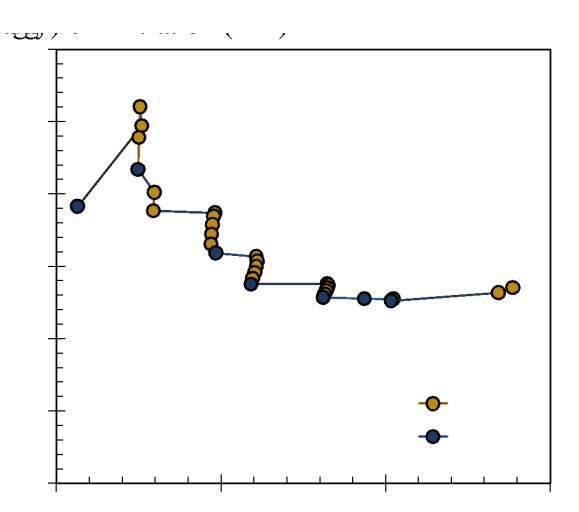
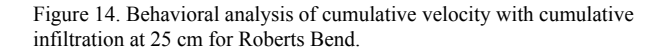


Figure 13. Behavioral analysis of deformation with volumetric water content for Roberts Bend at 25 cm.

Figure 14 shows the behavioral trend between the cumulative velocity (v_{cum}) and cumulative infiltration at 25 cm for Roberts Bend. The cumulative velocity is defined as the deformation rate at any day with respect to day zero (initial phase). Figure 14 shows parallel paths of drying and wetting phases. This again, is due to the coupled hydro-mechanical behavior observed for the slope. The Point A in the figure is the same reference point from Figure 13. The initial increase in the velocity during wetting is due to the slope movement from rest.





It can be seen from Figure 14 as the data progress towards wetting, the tendency of decreasing v_{cum} was getting lower. For example, the length of A_1A_2 , A_3A_4 and AA_5 were 0.028, 0.018 and 0.0015. This was an interesting observation to watch how the pattern of v_{cum} was changing with cumulative infiltration. After the Point A, the subsequent wetting paths started to move higher compared to the previous wetting paths. The reason can be further explained from Figure 18. Point A appears to be closer to the air entry value for 25 cm. Therefore, the soil at 25 cm reached near saturation at Point A. This resulted in a velocity increase following Point A in Figure 14. The 165 mm cumulative infiltration at point A is assumed to be the reason for the behavioral shift in Figure 14.

4.2 Hydro-Mechanical Behavioral Analysis at 44 cm

Figure 15 shows the behavioral analysis of deformation with volumetric water content for Roberts Bend at 44 cm. The deformation behavior followed different drying and wetting path with volumetric water content. The response was not as sharp as it had been at 25 cm (see Figure 13). This is expected as 44 cm is located deeper than 25 cm.

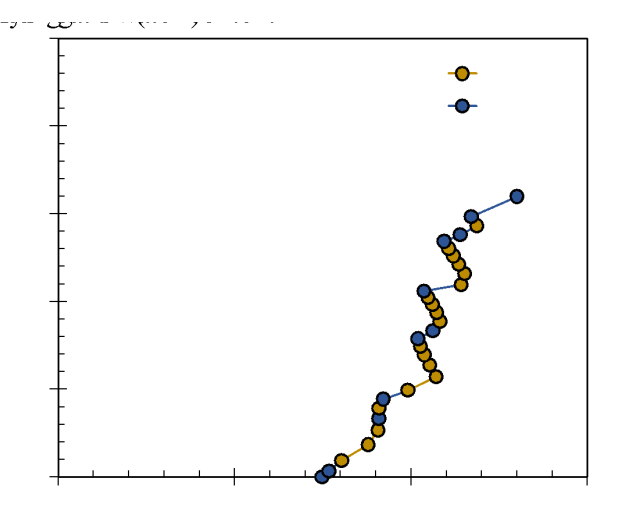


Figure 15. Behavioral analysis of deformation with volumetric water content for Roberts Bend at 44 cm.

In some phases, drying and wetting path seems to align. For example. DE is a wetting and EF is a drying path. At D, E and F the cumulative infiltration are 58.97 mm, 96.31 mm, and 95.56 mm, respectively. The cumulative infiltration increased from D to E by 64 percent. The cumulative infiltration dropped from E to F by 0.7 percent. The 0.7 percent drop of cumulative infiltration from E to F did not affect the trend to shift from DE path. Given that 44 cm is deeper than 25 cm, the 0.7 percent decrease in surface infiltration is likely to have a less noticeable effect on the hydrologic behavior at 44 cm than it is at 25 cm. Therefore, the drying path EF aligned with the wetting path DE. Upon reaching Point A, the volumetric water content at 44 cm was 0.46. The saturated volumetric water content at 44 cm was 0.52. Thus, the cumulative infiltration at Point A caused near saturation at 44 cm. As a result, the BC wetting path was steeper than the GA wetting path. Here, the slope of GA path was 1.74 mm per volumetric water content (average) and the slope of BC path was 4.83 mm per volumetric water content (average). The cumulative infiltration at A was 165 mm.

Figure 16 shows the behavioral analysis of the cumulative velocity with cumulative infiltration at 44 cm for Roberts Bend. The figure shows two initial wetting responses compared to the one initial wetting response for 25 cm from Figure 13. For example, from 1 to 2 in Figure 16, the 44 cm showed a wetting behavior. From 1 to 2, 25 cm demonstrated a drying behavior in Figure 13. The soil at 44 cm is deeper than the soil at 25 cm. Hence, rainfall and evapotranspiration response would be different for 25 cm than 44 cm. This has caused dissimilar response from 1 to 2 between 25 cm and 44 cm. Overall, the drying and wetting path for 44 cm from Figure 16 has shown identical trends alike 25 cm from Figure 14. Like Figure 14, the tendency of decreasing v_{cum} was getting lower with cumulative infiltration increase at 44 cm.



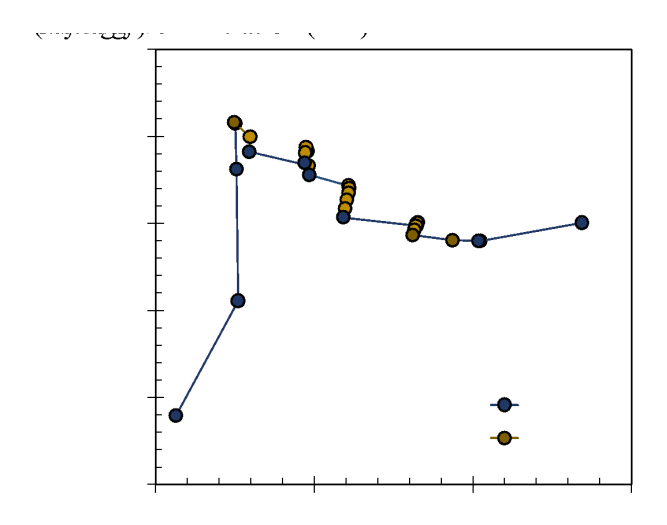


Figure 16. Behavioral analysis of cumulative velocity with cumulative infiltration at 44 cm for Roberts Bend.

From Figure 16, the length of A_1A_2 and AA_3 were 0.0073 and 0.0014, respectively. Upon reaching Point A, the v_{cum} path for 44 cm has shifted to move upwards. The Point A is the same reference point from 25 cm. This shift in v_{cum} path can be explained from Figure 17. Figure 17 presents the SWCCs from the FEM model at 25 cm and 44 cm depths.

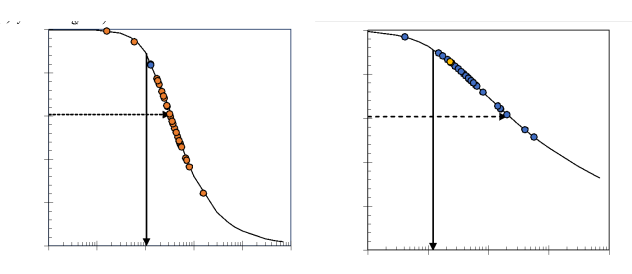


Figure 17. SWCC for Roberts Bend obtained from PLAXIS data: (a) data at 25 cm depth; (b) data at 44 cm depth.

The Point, A, in the figure appears to be close to the air entry value at 44 cm. Observing the path after Point A supports this supposition. In comparison to earlier stages, the trend began to shift upward. The effective degree of saturation was 0.855 at 44 cm, which corresponded to the air-entry value. The effective saturation degree associated with point A₄ was 0.89. As a result, after Point A, 44 cm has reached a wet state. A similar pattern was observed for 25 cm. As a result, overall analysis for 25 cm and 44 cm indicated that the path had changed behavior at 165 mm of cumulative infiltration. As a result of this shift, the hydro-mechanical behavior at 25 cm and 44 cm began to shift in a direction that resulted in saturation.

4.2.1 Changes in Mean Stress Driven by Changes in Suction Stress

Figure 18 shows the behavioral trend of mean effective stress (p') with suction stress (σ'_s) at 25 cm. The mean effective stress is defined as Equation 2

$$p' = \frac{\sigma'_{1} + 2\sigma'_{3}}{3} \tag{2}$$

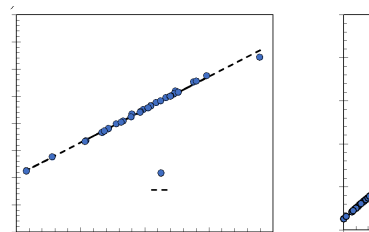
where, σ'_1 and σ'_3 are the major and minor principal stress, respectively. The mean effective stress is related with the volume changes of a soil. The mean effective stress concept has been effectively used in slope stability analysis several researchers (Oh and Lu 2015; Damiano et al. 2017; Summersgill et al. 2017). Further, suction stress was evaluated for the soil slope at the two depths of interest (i.e., 25 cm and 44 cm). The suction stress is the product of effective degree saturation and suction stress. The suction stress is a state variable in partially saturated soils that describes the net interparticle force generated within a matrix of unsaturated soil particles due to the combined effects of negative pore water pressure and surface tension. Suction stress is defined

$$\sigma'_{s} = S_{e} \psi \tag{3}$$

where, S_e = the effective degree of saturation = $\frac{(\theta - \theta_r)}{(\theta_s - \theta_r)}$; θ = the

FEM volumetric water content; and ψ = the FEM soil suction. For conditions in which the pore air pressure is assumed to be atmospheric pressure, suction stress can be directly obtained from PLAXIS as active pore pressure, p_{act} .

The suction stress is related to the hydrologic behavior of the soil. Thus, the effect of coupling hydrologic and mechanical behavior can be effectively analyzed using the combined action of the mean effective stress and the suction stress. Figure 18 shows a straight-line correlation between the mean effective stress and the suction stress at 25 cm and 44 cm.



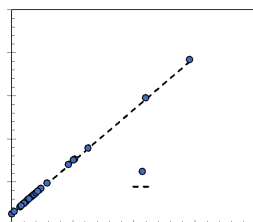


Figure 18. Behavioral analysis of mean effective stress with suction stress for Roberts Bend: (a) data at 25 cm depth; (b) data at 44 cm depth.

The general equation for the trendline on Figure 18(a) and Figure 18(b) can be translated as Equation 4,

$$p' = a\sigma'_{s} + b \tag{4}$$



where, a = the slope and b = the intercept. The intercept represents the mean effective stress at saturation (i.e., p' at $\sigma'_{s} = 0$), which is approximately 10.4 kPa at 25 cm and

approximately 12.7 kPa at 44 cm. The mean effective stress is an indicator of the confining pressure at a given depth and represents the initial saturation state of the system. When compared the SWCCs produced at each depth, as shown previously in Figure 17, it appears that the intercept (i.e., mean effective stress at saturation) corresponds to air-entry values, which are depth dependent. However, it was observed that the slope coefficient was constant for both 25 cm and 44 cm. The slope coefficient indicates the rate of change in the stress state of the hillslope system relative to the change in the hydrologic state. Thus, the slope value is a coupling factor that links mechanical behavior to hydrological of a hillslope system. It was hypothesized as the slope coefficient value of 0.608 might correlate with the inflection point on the SWCC for 25 cm and 44 cm as shown in Figure 17(a) and Figure 17(b). Thus, Equation 4 provides a simple mean to describe the coupled hydro-mechanical behavior of a hillslope system.

5 CONCLUSION

The goal of this paper was to examine the behavior of an actual monitored slope during a month of wetting season. Both rainfall and evapotranspiration were considered during the wetting season. The investigation was carried out at two different depths within a monitored site. The near-surface locations served as the site's actual recorded monitoring stations. The slope experienced a behavioral shift at 165 mm of cumulative infiltration, according to the behavioral analysis at the recorded locations. The soil reached near saturation from dry at 25 cm and 44 cm. As a result, the 165 mm cumulative infiltration may be seen as a point at which the slope's hydrologic and mechanical behavior can be discerned. At the recorded sites, the behavioral analysis between soil suction stress and soil mean effective stress was also examined. The mean effective stress is related to the state of volume change in a soil. The suction stress is linked to the soil's hydrologic behavior. Thus, suction stress and mean effective stress were analyzed together to assess the coupled hydro-mechanical behavior. A straight-line regression form resulted from the behavioral study between the mean effective stress and the suction stress. The slope of the regression line was assumed to be linked to the inflection point of a SWCC at the appropriate depth. The intercept of the regression equation was assumed to be represented by the air entry value. However, it is acknowledged that these observations are for one slope system. Further study will be needed to see whether this hypothesis holds true for various slopes. Also, the soil in both layers was considered to have no hysteresis throughout the current research. In addition, root uptake/intake and root strength were not considered in the analysis. Therefore, soil root considerations and soil hysteresis can be incorporated into future rainfall-induced slope behavioral analysis study.

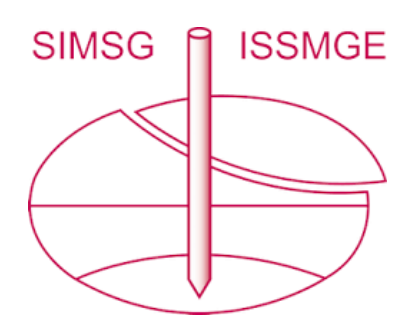
6 REFERENCES

- Ahmed, F. S., Bryson, L. S., and Crawford, M. M. (2021). "Prediction of seasonal variation of in-situ hydrologic behavior using an analytical transient infiltration model." Engineering Geology, 294, 106383.
- Baum, R. L., Savage, W. Z., and Godt, J. W. (2008). "TRIGRS-A Fortran program for transient rainfall infiltration and grid-based regional slope-stability analysis, version 2.0: U.S. Geological Survey Open-File Report". US Geological Survey Open-File Report, 2008-1159, 75p.
- Brinkgreve, R., Kumarswamy, S., Swolfs, W., Waterman, D., Chesaru, A., and Bonnier, P. (2016). "PLAXIS 2016." PLAXIS by, The Netherlands
- Crawford, M. M., Bryson, L. S., Woolery, E. W., and Wang, Z. (2019).
 "Long-term landslide monitoring using soil-water relationships and electrical data to estimate suction stress." Engineering Geology, 251, 146-157.
- Crawford, M. M., Bryson, L. S., Woolery, E. W., and Wang, Z. (2018). "Using 2-D electrical resistivity imaging for joint geophysical and geotechnical characterization of shallow landslides." Journal of Applied Geophysics, 157, 37-46.
- Distefano, P., Peres, D. J., Scandura, P., and Cancelliere, A. (2022). "Brief communication: Introducing rainfall thresholds for landslide triggering based on artificial neural networks." Natural Hazards and Earth System Sciences, 22(4), 1151-1157.
- Ering, P., and Babu, G. S. (2016). "Probabilistic back analysis of rainfall induced landslide-A case study of Malin landslide, India." Engineering Geology, 208, 154-164.
- Gao, L., Zhang, L. M., and Chen, H. (2017). "Likely scenarios of natural terrain shallow slope failures on Hong Kong Island under extreme storms." Natural Hazards Review, 18(1), B4015001.
- Hoang, N.-D., and Bui, D. T. (2018). "Spatial prediction of rainfall-induced shallow landslides using gene expression programming integrated with GIS: a case study in Vietnam." Natural Hazards, 92(3), 1871-1887.
- Hu, R., Hong, J.-M., Chen, Y.-F., and Zhou, C.-B. (2018). "Hydraulic hysteresis effects on the coupled flow-deformation processes in unsaturated soils: Numerical formulation and slope stability analysis." Applied Mathematical Modelling, 54, 221-245.
- Iverson, R. M. (2000). "Landslide triggering by rain infiltration." Water resources research, 36(7), 1897-1910.
- Kim, S. W., Chun, K. W., Kim, M., Catani, F., Choi, B., and Seo, J. I. (2021). "Effect of antecedent rainfall conditions and their variations on shallow landslide-triggering rainfall thresholds in South Korea." Landslides, 18(2), 569-582.
- Liu, X., and Wang, Y. (2021). "Probabilistic simulation of entire process of rainfall-induced landslides using random finite element and material point methods with hydro-mechanical coupling." Computers and Geotechnics, 132, 103989.
- Marin, R. J., and Velásquez, M. F. (2020). "Influence of hydraulic properties on physically modelling slope stability and the definition of rainfall thresholds for shallow landslides." Geomorphology, 351, 106976.
- Montrasio, L., and Valentino, R. (2008). "A model for triggering mechanisms of shallow landslides." Natural Hazards and Earth System Sciences, 8(5), 1149-1159.
- Mualem, Y. (1976). "A new model for predicting the hydraulic conductivity of unsaturated porous media." Water resources research, 12(3), 513-522.
- Oh, S., and Lu, N. (2015). "Slope stability analysis under unsaturated conditions: Case studies of rainfall-induced failure of cut slopes." Engineering Geology, 184, 96-103.
- Rana, H., and Babu, G. (2022). "Regional back analysis of landslide events using TRIGRS model and rainfall threshold: an approach to estimate landslide hazard for Kodagu, India." Bulletin of Engineering Geology and the Environment, 81(4), 1-16



- Schulz, W. H., Smith, J. B., Wang, G., Jiang, Y., and Roering, J. J. (2018). "Clayey landslide initiation and acceleration strongly modulated by soil swelling." Geophysical Research Letters, 45(4), 1888-1896.
- Soga, K., Alonso, E., Yerro, A., Kumar, K., and Bandara, S. (2016).
 "Trends in large-deformation analysis of landslide mass movements with particular emphasis on the material point method."
 Géotechnique, 66(3), 248-273.
- Tang, Y., Wu, W., Yin, K., Wang, S., and Lei, G. (2019). "A hydro-mechanical coupled analysis of rainfall induced landslide using a hypoplastic constitutive model." Computers and Geotechnics, 112, 284-292.
- Tang, Y., Yin, K.-l., Liu, L., Zhang, L., and Fu, X.-l. (2017). "Dynamic assessment of rainfall-induced shallow landslide hazard." Journal of Mountain science, 14(7), 1292-1302.
- Wei, X., Fan, W., Cao, Y., Chai, X., Bordoni, M., Meisina, C., and Li, J. (2020). "Integrated experiments on field monitoring and hydro-mechanical modeling for determination of a triggering threshold of rainfall-induced shallow landslides. A case study in Ren River catchment, China." Bulletin of Engineering Geology and the Environment, 79(1), 513-532.
- Wildenschild, D., Hopmans, J., and Simunek, J. (2001). "Flow rate dependence of soil hydraulic characteristics." Soil Science Society of America Journal, 65(1), 35-48.
- Wu, L., Zhang, L. M., Zhou, Y., Xu, Q., Yu, B., Liu, G., and Bai, L. (2018). "Theoretical analysis and model test for rainfall-induced shallow landslides in the red-bed area of Sichuan." Bulletin of Engineering Geology and the Environment, 77(4), 1343-1353.
- Wu, L., Zhu, S., and Peng, J. (2020). "Application of the Chebyshev spectral method to the simulation of groundwater flow and rainfall-induced landslides." Applied Mathematical Modelling, 80, 408-425.
- Yang, K.-H., Nguyen, T. S., Rahardjo, H., and Lin, D.-G. (2020).
 "Deformation characteristics of unstable shallow slopes triggered by rainfall infiltration." Bulletin of Engineering Geology and the Environment, 80(1), 317-344.
- Yang, K.-H., Nguyen, T. S., Rahardjo, H., and Lin, D.-G. (2020)
 "Deformation Characteristics with Porewater Pressure Development of Shallow Landslide Triggered by Rainfall Infiltration." Workshop on World Landslide Forum, Springer, 227-234.
- Yang, K.-H., Uzuoka, R., Lin, G.-L., and Nakai, Y. (2017). "Coupled hydro-mechanical analysis of two unstable unsaturated slopes subject to rainfall infiltration." Engineering Geology, 216, 13-30.
- Yuniawan, R. A., Rifa'i, A., Faris, F., Subiyantoro, A., Satyaningsih, R., Hidayah, A. N., Hidayat, R., Mushthofa, A., Ridwan, B. W., and Priangga, E. (2022). "Revised Rainfall Threshold in the Indonesian Landslide Early Warning System." Geosciences, 12(3), 129.
- Zhan, T. L., Jia, G., Chen, Y. M., Fredlund, D., and Li, H. (2013). "An analytical solution for rainfall infiltration into an unsaturated infinite slope and its application to slope stability analysis." International Journal for Numerical and Analytical Methods in Geomechanics, 37(12), 1737-1760.
- Zhang, M., Yang, L., Ren, X., Zhang, C., Zhang, T., Zhang, J., and Shi, X. (2019). "Field model experiments to determine mechanisms of rainstorm-induced shallow landslides in the Feiyunjiang River basin, China." Engineering Geology, 262, 105348.
- Zhuang, J., Peng, J., Wang, G., Iqbal, J., Wang, Y., Li, W., Xu, Q., and Zhu, X. (2017). "Prediction of rainfall-induced shallow landslides in the Loess Plateau, Yan'an, China, using the TRIGRS model." Earth Surface Processes and Landforms, 42(6), 915-927.

INTERNATIONAL SOCIETY FOR SOIL MECHANICS AND GEOTECHNICAL ENGINEERING



This paper was downloaded from the Online Library of the International Society for Soil Mechanics and Geotechnical Engineering (ISSMGE). The library is available here:

https://www.issmge.org/publications/online-library

This is an open-access database that archives thousands of papers published under the Auspices of the ISSMGE and maintained by the Innovation and Development Committee of ISSMGE.

The paper was published in the proceedings of the 17th Pan-American Conference on Soil Mechanics and Geotechnical Engineering (XVII PCSMGE) and was edited by Gonzalo Montalva, Daniel Pollak, Claudio Roman and Luis Valenzuela. The conference was held from November 12th to November 16th 2024 in Chile.